The Astrophysical Journal, 861:17 (9pp), 2018 July 1 https://doi.org/10.3847/1538-4357/aac9bf

Quantum-vibrational-state-selected Integral Cross Sections and Product Branching Ratios for the Ion-molecule Reactions of $N_2^+(X^2\Sigma_g^+;\ v^+ = 0\text{–}2) + H_2O$ and $H_2O^+(X^2B_1:\ v_1^+v_2^+v_3^+ = 000$ and $100) + N_2$ in the Collision Energy Range of 0.04–10.00 eV

Yuntao Xu, Bo Xiong, Yih Chung Chang, and Cheuk-Yiu Ng
Department of Chemistry, University of California, Davis, Davis, CA 95616, USA; cyng@ucdavis.edu
Received 2018 March 23; revised 2018 May 13; accepted 2018 May 30; published 2018 June 27

Abstract

By combining the vacuum ultraviolet laser pulsed field ionization-photoion (VUV-PFI-PI) ion source with the double quadruple-double octopole (DQDO) ion-guided mass spectrometer, we have investigated the center-of-mass collision energy (E_{cm}) and vibrational-state dependences of the ion-molecule reactions of $N_2^+(X^2\Sigma_g^+:\ v^+ = 0\text{–}2) + H_2O$ and $H_2O^+(X^2B_1:\ v_1^+v_2^+v_3^+ = 000$ and $100) + N_2$ covering the E_{cm} range of 0.04–10.00 eV. The absolute integral cross sections (σ's) for the charge transfer (CT) [$\sigma_{CT}(v^+)$] channel to form H_2O^+ and the H-atom transfer (HT) [$\sigma_{HT}(v^+)$] channel to form N_2H^+ from the $N_2^+(X^2\Sigma_g^+:\ v^+ = 0\text{–}2) + H_2O$ reactions have been determined, revealing the dominance of $\sigma_{CT}(v^+)$ over $\sigma_{HT}(v^+)$ at $E_{cm} = 0.04\text{–}8.00$ eV. The E_{cm} dependence of $\sigma_{CT}(v^+)$ at low $E_{cm} < 1.00$ eV is consistent with the long-range ion-dipole and ion-induced dipole CT mechanism. Minor vibrational inhibition is observed for the $\sigma_{CT}(v^+)$ at low $E_{cm} \leqslant 0.30$ eV, which can be rationalized by the near-resonance CT mechanism. While the $\sigma_{HT}(v^+)$ values are consistent with previous measurements, the $\sigma_{CT}(v^+)$ obtained here resolve a hump at $E_{cm} = 1.0\text{–}5.0$ eV, which is not observed previously. This feature is attributed to the formation of excited $H_2O^+(B^2B_2)$ ions via the collision-assisted CT mechanism. The branching ratio for product H_2O^+[BR(H_2O^+)] is found to be constant (0.82 ± 0.05) at $E_{cm} = 0.04\text{–}1.00$ eV, and is independent of v^+ vibrational state. As E_{cm} is increased from 1.0 eV, the BR(H_2O^+) reaches a maximum of 0.93 at $E_{cm} \approx 3.00$ eV, followed by the decline to 0.20 at $E_{cm} \geqslant 9.0$ eV, where $\sigma_{HT}(v^+)$ becomes dominant compared to $\sigma_{CT}(v^+)$. The $\sigma_{PT}(v_1^+v_2^+v_3^+)$ for the formation of N_2H^+ via the proton transfer (PT) channel of the $H_2O^+(X^2B_1$: 000 and 100) + N_2 reaction has also been measured. The comparison of the σ_{PT}(000 and 100) values reveals significant (100) vibrational enhancement. Furthermore, the E_{cm} thresholds determined here for σ_{PT}(000 and 100) are in agreement with their thermochemical thresholds. The BR and σ values determined here are valuable for modeling the ion chemistry occurring in planetary atmospheres, in addition to serving as benchmarks for state-of-the-art quantum dynamics calculations.

Key words: astrochemistry – molecular processes – planets and satellites: atmospheres

1. Introduction

Nitrogen (N_2) and water (H_2O) molecules and their cations (N_2^+ and H_2O^+) are some of the main molecular species in planetary atmospheres and astrochemical environments, where chemical reactions involving N_2^+/N_2 and H_2O^+/H_2O play an important role in determining the chemical compositions as well as the chemical evolutions (Giguere & Huebner 1978; Huntress et al. 1980; Semo & Koski 1984; Smith 1992; Smith & Spanel 1995; Herbst 2001; Williams et al. 2002; Snow & Bierbaum 2008; Larsson et al. 2012). Since N_2^+ and H_2O^+ cations are mostly produced by electron impact and solar vacuum ultraviolet (VUV) photoionization of atmospheric N_2 and H_2O neutrals, long-lived rovibronically excited N_2^+ and H_2O^+ ions are expected to be produced in abundance in planetary environments. We have pointed out previously that long-lived N_2^+ and H_2O^+ ions thus produced in different quantum states can have different chemical reactivity toward the same neutral reactants (Chang et al. 2012; Xu et al. 2013b). Hence, it is highly desirable to take into account quantum-rovibronic-state effects on σ values of relevant ion-molecule reactions involving N_2^+ and H_2O^+ ions in order to achieve realistic modeling of the chemistry occurring in planetary atmospheres and astrochemical environments.

Most ion-molecule reactions of relevance to astrophysics are known to take place at near thermal energies with center-of-mass collision energies of $E_{cm} \leqslant 30\text{–}40$ meV. However, supra-thermal ion-molecule collisions in the E_{cm} range of a few eV also occur. In such cases, reactants may originate from solar VUV or electron impact photodissociation and photoionization processes with high kinetic energy releases. Dressler and coworkers have shown that the fluorescence glow observed near the surface of the space shuttle during its exit of or entry into the Earth's atmosphere can involve supra-thermal reactions of $N_2^+ + H_2O$ (Dressler et al. 1990a). After taking into account of the velocities of space vehicles, ion-molecule collisions between N_2^+ and H_2O associated with contaminant clouds of the space vehicles can reach supra-thermal energies of a few eV.

With the goal to establish a reliable database of quantum-state-selected σ values for chemical modeling of planetary atmospheres, we have developed unique ion-molecule reaction facilities for ion-molecule collisional studies. By combining the vacuum ultraviolet laser pulsed field ionization-photoion (VUV-PFI-PI) ion source with the DQDO radio-frequency (rf) ion-guided mass spectrometer (Chang et al. 2011, 2012), we have recently succeeded in recording σ values for an array of quantum-rovibronic-state-selected ion-molecule reactions in the E_{cm} range of 0.03–10.00 eV, which are relevant to chemical modeling of planetary atmospheres. These reactions include $N_2^+(X^2\Sigma_g^+:\ v^+ = 0\text{–}2;\ N^+ = 0\text{–}9) + Ar$ (CH_4, C_2H_2); $H_2O^+(X^2B_1:\ v_1^+v_2^+v_3^+ = 000,\ 020,\ 100;\ N^+_{Ka+Kc+} = 0_{00} -$

3_{22}) + H_2 (HD, D_2, CO); $H_2^+(X^2\Sigma_g^+$: $v^+ = 1$–3; $N^+ = 0$–3) + Ne; and $O_2^+(a^4\Pi_{u5/2,3/2,1/2,-1/2}$: $v^+ = 1$–2; J^+) [$O_2^+(X^2\Pi_{g3/2,1/2}$: $v^+ = 22$–23; J^+)] + Ar. (Chang et al. 2011, 2012; Xu et al. 2012, 2016, 2017a, 2017b, 2013a, 2013b; Li et al. 2014; Song et al. 2016; Xiong et al. 2017a, 2017b). The current vibrational state-selected σ-measurements on the $N_2^+(X^2\Sigma_g^+$: $v^+ = 0$–2; N^+) + H_2O and $H_2O^+(X^2B_1$: $v_1^+v_2^+v_3^+ = 000$ and 100; $N^+{}_{Ka+Kc}$) + N_2 reactions represent a continuation of this effort. In addition to providing reliable quantum-state-selected cross sections for chemical modeling, which are mostly not available previously, the σ values and product branching ratios (BRs) obtained here can also serve as valuable benchmarks for first-principle theoretical quantum reaction dynamics calculations.

Because of the importance of the $N_2^+ + H_2O$ reaction, many kinetic and dynamic studies on this reaction have been reported in past decades (Shahin 1967; Turner & Rutherford 1968; Howard et al. 1970; Dreyer & Perner 1971; Bolden & Twiddy 1972; Howorka et al. 1974; Karpas et al. 1978; Smith et al. 1978; Tichý et al. 1979; Huntress et al. 1980; Parent et al. 1985; Dressler et al. 1990b, 1993; Yuan et al. 2011). However, as shown below, previous reported σ values and those σ values converted from rate constants (k_rs) are widely scattered and lack the general agreement. These large deviations, particularly those observed between different kinetics studies at low E_{cm} values, have motivated this study, aiming to reexamine the σ values and product BRs of this reaction. According to previous experimental studies, the $N_2^+(v^+ = 0$–2) + H_2O reaction has two major product channels. Reactions (1) and (2) list the respective heats of reaction (ΔE) of −2.963 and −1.911 eV for the formations of H_2O^+ and N_2H^+ by the $N_2^+(X^2\Sigma_g^+$: $v^+ = 0$) + H_2O reaction (Ruscic et al. 2013),

$$N_2^+(X^2\Sigma_g^+;\ v^+ = 0) + H_2O \rightarrow H_2O^+ + N_2 \quad \Delta E = -2.963 \pm 0.001\ \text{eV} \tag{1}$$

$$\rightarrow N_2H^+ + OH \quad \Delta E = -1.911 \pm 0.001\ \text{eV}. \tag{2}$$

The ΔE values for the $N_2^+(v^+ = 1$ and 2) + H_2O reactions can be calculated using the respective vibrational energies of 2181 and 4312 cm^{-1}. Here, the σ values for the formation of H_2O^+ via the charge transfer (CT) and N_2H^+ via the H-atom transfer (HT) product channels are referred to as $\sigma_{CT}(v^+)$ and $\sigma_{HT}(v^+)$, respectively. The most interesting observation of this study is the hump at $E_{cm} = 1.0$–5.0 eV resolved in the $\sigma_{CT}(v^+ = 0$–2) curves [$\sigma_{CT}(v^+ = 0$–2) versus E_{cm}], which was not observed in previous measurements. As discussed below, this feature is tentatively attributed to the formation of the $H_2O^+(B\ ^2B_2)$ excited state via the collision-assisted near-resonance CT mechanism.

We also reported on σ-measurements for the $H_2O^+(X^2B_1$: $v_1^+v_2^+v_3^+ = 000$ and 100) + N_2 reactions at $E_{cm} = 0.30$–8.00 eV, which can be considered the reverse reaction of reaction (1). In the E_{cm} range of 0.04–10.0 eV, we have only observed and determined the $\sigma_{PT}(v_1^+v_2^+v_3^+)$ values for formation of N_2H^+ via the proton transfer (PT) channel of the $H_2O^+(X^2B_1$: 000 and 100) + N_2 reaction. The PT channel shown in reaction (3) is known to be endothermic with $\Delta E = 1.05 \pm 0.01$ eV, when reactant $H_2O^+(X^2B_1)$ ion is prepared in the ground (000) vibrational state,

$$H_2O^+(X^2B_1\text{: 000}) + N_2 \rightarrow N_2H^+ + OH \quad \Delta E = 1.05 \pm 0.01\ \text{eV}. \tag{3}$$

For reactant $H_2O^+(X^2B_1)$ ion prepared in the (100) symmetric stretching vibrational state, the ΔE value is known to be 0.65 ± 0.01 eV. Other endothermic product channels, such as the formation of $N_2^+ + H_2O$ in the collision of $H_2O^+(X^2B_1$: 000 and 100) + N_2, are too weak to be measured. Although the σ_{PT}(000 and 100) values are low, we are still able to measure the σ_{PT}(000 and 100) curves. The comparison of these curves reveals strong vibrational enhancement for excitation of the (100) symmetric stretching vibrational mode of reactant $H_2O^+(X^2B_1)$ ion. Furthermore, the σ_{PT}(000 and 100) curves observed here exhibit distinct E_{cm} thresholds, which are found to be in accord with their thermochemical thresholds.

2. Experiment

The VUV-PFI-PI DQDO ion-molecule reaction apparatus and experimental procedures employed in this study have been described in detail previously (Chang et al. 2012; Xu et al. 2013b; Xiong et al. 2017a). This apparatus consists of a molecular beam source for the generation of a pulsed supersonic N_2 (H_2O) beam, a VUV laser PFI-PI ion source for the preparation of quantum-state-selected reactant $N_2^+(X^2\Sigma_g^+$; $v^+ = 0$–2; N^+) [$H_2O^+(X^2B_1$: $v_1^+v_2^+v_3^+ = 000$ and 100; $N^+{}_{Ka+Kc+} = 0_{00}$)] ions with narrow laboratory kinetic energy (E_{lab}) spreads ($\Delta E_{lab} \approx \pm 0.05$ eV), and a DQDO mass spectrometer for σ measurements. A set of dual rf-octopole ion guides was used for guiding the reactant and product ions in and out of the reactant gas cell. The measurements of reactant and product ion intensities were made by using the product quadrupole mass spectrometer (QMS) along with a Daly-type ion detector.

For the $N_2^+(X^2\Sigma_g^+$; $v^+ = 0$–2) + H_2O [$H_2O^+(X^2B_1$: $v_1^+v_2^+v_3^+ = 000$ and 100) + N_2] reaction study, the tunable VUV laser radiation was generated by resonance-enhanced four-wave sum-frequency ($2\omega_1 + \omega_2$) mixing schemes using a Kr (Xe) jet as the nonlinear medium. The fundamental frequencies ω_1 and ω_2 were generated by two independently tunable dye lasers pumped by an identical Nd:YAG laser operated at 15 Hz. While the laser ω_1 output was set to match the $5p \leftarrow 4p$ ($6p \leftarrow 5p$) resonance-enhanced two-photon transition of Kr (Xe) atom, the laser ω_2 output was scanned to generate the VUV ($2\omega_1 + \omega_2$) sum-frequency range required for the experiment, i.e., photoionizing N_2 (H_2O) molecules into selected quantum rovibrational states of $N_2^+(X^2\Sigma_g^+$; $v^+ = 0$–2) [$H_2O^+(X^2B_1$: 000 and 100)] reactant ions.

We introduce the precursor N_2 (H_2O) molecules into the photoionization/photoexcitation (PI/PEX) region in the form of a supersonic molecular beam, traveling along the central axis of the DQDO mass spectrometer to intersect the VUV laser beam perpendicularly at the PI/PEX center. By employing the sequential electric field pulse scheme to generate VUV-PFI-PIs, we achieved narrow kinetic energy spreads ($\Delta E_{lab} \approx \pm 0.05$ eV) as well as high detection sensitivity for VUV-PFI-PIs. The most essential elements of the VUV-PFI-PI ion source consist of three ion lenses, E1, I1, and I2, where the space between E1 and I1 defines the PI/PEX region; and I2 is the ion lens used to block out the prompt ions from exiting the ion

source. The high-n Rydberg neutral species $N_2^*(n)$ [$H_2O^*(n)$] as well as prompt N_2^+ (H_2O^+) ions are produced by VUV laser excitation of the N_2 (H_2O) molecular beam at the PI/PEX center, where n represents the principal quantum number. At a delay of 100 ns with respect to the VUV laser pulse, the first electric field pulse [amplitude = 2 V/cm, duration = 2 μs] is applied at lens I1. This first electric field pulse serves to retard and thus separate the prompt ions spatially from the neutral $N_2^*(n)$ [$H_2O^*(n)$] Rydberg species. At a delay of 300 ns with respect to the termination of the separation electric field pulse, the second electric field pulse (amplitude = 14 V/cm, duration = 0.5 μs) is applied to lens E1. This second electric field pulse serves to PFI neutral $N_2^*(n)$ [$H_2O^*(n)$] Rydberg species, and to extract PFI-PIs thus formed along with prompt ions out of the PI/PEX region, traveling toward the rf-octopole reaction gas cell. Since the prompt ions have lower kinetic energies than that of the PFI-PIs because of the prompt ion retarding effect, we were able to apply a potential energy barrier at lens I2 to cleanly block out the prompt ions, passing only the PFI-PIs to the reaction gas cell. This capability allows the quantum-rovibronic-state-selection of small molecular ions, such as N_2^+ and H_2O^+, with essentially 100% purity. The key for achieving high kinetic energy resolution (i.e., narrow ΔE_{lab} spread) for the PFI-PIs is to turn off the second electric field pulse before the PFI-PIs exit the PI/PEX region, such that all PFI-PIs produced in the PI/PEX region gain the same momentum. In this study, for each PFI-PI vibrational band, N_2^+ ions were prepared by setting the VUV laser sum-frequency at the strongest rotational peak position, i.e., the Q branch. Thus, the vibrationally selected $N_2^+(v^+ = 0–2; N^+)$ VUV-PFI-PIs are in a distribution of low $N^+ = 0–9$ rotational states. (Chang et al. 2012) For the PFI-PI $H_2O^+(X^2B_1$: 000 and 100) vibrational bands, single 0_{00}, 1_{11}, and 2_{11} rotational states are also selected. However, no observable rotational effects are found for the σ values of the $H_2O^+(X^2B_1$: 000 and 100) + N_2 reactions.

The reaction gas cell is situated between the first and second rf-octopoles, such that slow CT product H_2O^+ ions can be effectively extracted out of the reaction gas cell by applying a small dc electric field between the two rf-octopoles. In this study, we fill the neutral H_2O (N_2) reactant gas in the rf-octopole reaction gas cell in the pressure range from 1.0×10^{-5} to 1.0×10^{-4} Torr as monitored by an MKS Baratron. After passing through the reaction gas cell, the intensity of the attenuated reactant N_2^+ (H_2O^+) PFI-PI beam is measured by the product QMS. Product ions resulting from the collisions between the PFI-PI beam and neutral reactant molecules in the reaction gas cell are also guided into the product QMS for intensity measurements. The ion intensities thus measured allow the determination of σ values for the ion-molecule reactions of interest based on the Beer–Lambert Law.

We have pointed out in previous studies (Xu et al. 2012, 2013b, 2017a, 2017b) that in an ion-beam gas cell study, such as in this experiment, the thermal motions of neutral H_2O (N_2) molecules in the reaction gas cell can be the main contribution to the uncertainty of E_{cm} (i.e., ΔE_{cm}; Chantry 1971). For the reaction of $N_2^+(v^+ = 0–2) + H_2O$ [H_2O^+ (000 and 100) + N_2], the estimated uncertainties for $E_{cm} = 0.05$, 0.10, and 0.5 eV are 0.09, 0.13, and 0.29 eV (0.07, 0.10, and 0.23 eV), respectively. The ΔE_{cm} spreads have the effect of smoothing the integral cross section curves, particularly at low E_{cm} values; but the general trends for the σ curves are not expected to be seriously affected. For the conversion of E_{lab} into E_{cm}, we use the formula $E_{cm} = E_{lab} \times [M/(m^+ + M)]$, where m^+ and M represent the mass of the reactant ion and that of the neutral molecule, respectively.

All σ values presented in this study are based on the average of at least three independent and reproducible measurements. The standard deviations are generally 5%–10%, which represent the reproducibility of independent measurements. However, the systematic error limits for absolute σ determinations are significantly larger due to the lack of accurate calibration parameters used as well as the variation of experimental conditions and procedures used in different individual experiments. The σ values presented here have been calibrated to those determined previously for the formation of ArD^+ (ArH^+) from the $Ar^+_{3/2,1/2} + D_2$ ($Ar^+_{3/2,1/2} + H_2$) reactions (Tanaka et al. 1981; Ervin & Armentrout 1985; Qian et al. 2003); and we have assigned error limits of ≈30% (Chang et al. 2012; Xu et al. 2013b) for the absolute values of $\sigma_{CT}(v^+ = 0–2)$, $\sigma_{HT}(v^+ = 0–2)$, $\sigma_{PT}(000)$, and $\sigma_{PT}(100)$.

The $N_2^+(X^2\Sigma_g^+; v^+) + H_2O$ reaction was found to have only two opened product channels corresponding to the formation of H_2O^+ and N_2H^+. The BRs for H_2O^+ [$BR(H_2O^+)$] and N_2H^+ [$BR(N_2H^+)$] are determined here as $I(H_2O^+)/[I(H_2O^+) + I(N_2H^+)]$ and $I(N_2H^+)/[I(N_2H^+) + I(N_2H^+)]$, respectively, where $I(H_2O^+)$ and $I(N_2H^+)$ represent the intensities for product H_2O^+ and N_2H^+ ions Since $I(H_2O^+)$ and $I(N_2H^+)$ can be measured simultaneously, the error limits achieved for $BR(H_2O^+)$ and $BR(N_2H^+)$ measurements are generally about 5%. The definition of $BR(H_2O^+)$ and $BR(N_2H^+)$ gives the sum $BR(H_2O^+) + BR(N_2H^+)$ to be unity.

3. Results and Discussion

The current σ and BR measurements are mainly concerned with the $N_2^+(X^2\Sigma_g^+; v^+ = 0–2) + H_2O$ reaction. The inclusion of the σ measurement of the $H_2O^+(X^2B_1$: 000 and 100) + N_2 reaction is aimed to gain additional insight into the reaction mechanisms of the ion-molecule reaction system involving the neutral and ionic species N_2^+/N_2 and H_2O^+/H_2O.

3.1. $N_2^+(X^2\Sigma_g^+; v^+ = 0–2) + H_2O$

Mass Spectra: Figures 1(a) and (b) depict the respective mass spectra in the mass-to-charge ratio (m/z) range of 12–50 for the ion-molecule reaction of $N_2^+(X^2\Sigma_g^+; v^+ = 0) + H_2O$ at $E_{cm} = 0.40$ eV observed without and with H_2O gas filled in the rf-octupole reaction gas cell. Without H_2O filled in the reaction gas cell, the mass spectrum of Figure 1(a) reveals only two ion peaks at $m/z = 28$ and 29 with the intensity ratio of $I(m/z = 29):I(m/z = 28) = 0.0074$. Since this ratio is in excellent accord with that deduced using the known natural isotope abundances of $^{15}N/^{14}N$, the observed ion peaks at $m/z = 28$ and 29 can be confidently assigned as $^{14}N^{14}N^+$ and $^{15}N^{14}N^+$ ions, respectively.

When the gas cell is filled by neutral reactant H_2O gas at a pressure of 4.0×10^{-5} Torr, two additional ion peaks at $m/z = 18$ and 19 are discernible in the mass spectrum of Figure 1(b). The ion peak at $m/z = 18$ is assigned to H_2O^+ ions formed by the CT reaction (1), whereas the ion peak at $m/z = 19$ is identified as H_3O^+ ions formed by secondary

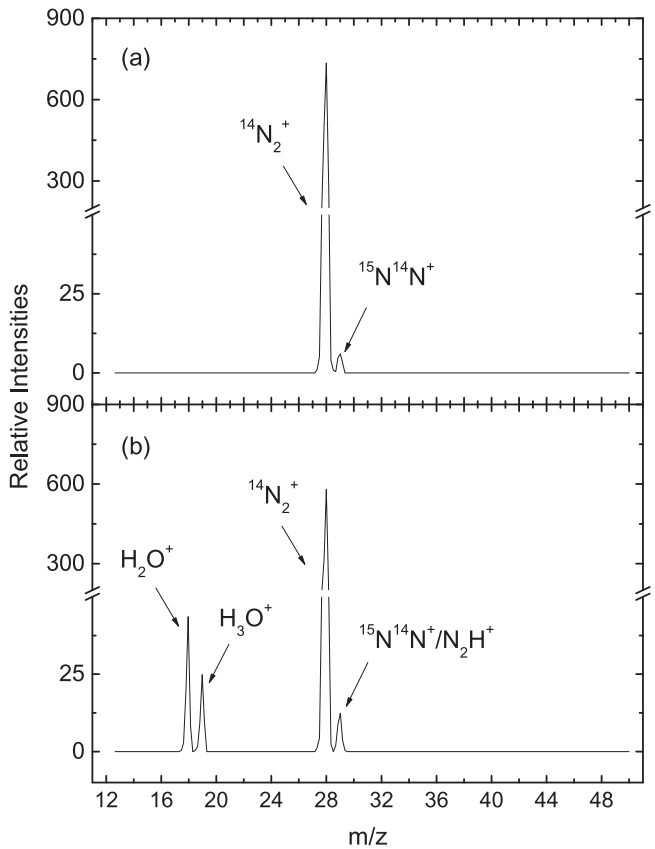

Figure 1. Comparison of the mass spectra with and without the neutral H_2O reactant. (a) Mass spectrum of the $N_2^+(v^+ = 0)$ reactant ion beam. Two peaks are observed at the position of $m/z = 28$ and 29, which are assigned as the $^{14}N_2^+$ and its isotopic form $^{15}N^{14}N^+$, respectively; and (b) mass spectrum observed for the reaction of $N_2^+(v^+ = 0) + H_2O$. Four peaks at $m/z = 18$, 19, 28, and 29 are observed, which are identified as the H_2O^+, H_3O^+, $^{14}N_2^+$, $^{15}N^{14}N^+$, and N_2H^+ ions. The last two ion species have the same m/z ratio. The pressure of the H_2O vapor in the gas cell is kept as 4×10^{-5} Torr. Both spectra are recorded at $E_{cm} = 0.40$ eV.

reactions between CT H_2O^+ ions and neutral H_2O molecules in the reaction gas cell. Because of the nature of long-range CT reaction mechanism, primary CT H_2O^+ ions formed by reaction (1) in the reaction gas cell are mostly slow ions with near thermal energies. These slow CT H_2O^+ ions have very high reaction rates for the formation of secondary H_3O^+ ions by $H_2O^+ + H_2O$ collisions in the reaction gas cell. For this reason, we have determined the actual intensity for CT product H_2O^+ ions by the sum of the observed intensities for H_2O^+ and H_3O^+ ions.

The $I(m/z = 29)$ of Figure 1(b) is higher than that observed in Figure 1(a), indicating that N_2H^+ ions are also produced in the $N_2^+ + H_2O$ collisions via the HT reaction (2). By combining the $I(m/z)$ measurements of Figures 1(a) and (b), we can correct for the contribution of isotropic $^{15}N^{14}N^+$ ions and obtain the actual intensity of product N_2H^+ ions. Without filling H_2O vapor in the reaction gas cell, we have carefully examined the intensity ratio of $I(m/z = 29)$:$I(m/z = 28)$ as a function of E_{cm} in the range of 0.05–10.0 eV, and we found that this ratio remains constant at 0.0074 throughout this E_{cm} range. This observation shows that the $^{15}N^{14}N^+$ ion intensity correction for product N_2H^+ ion can be reliably determined based on the $I(m/z = 28$ and 29) measurements with H_2O filled in the reaction gas cell, along with the isotopic ratio $I(m/z = 29)$:$I(m/z = 28)$ of 0.0074 calculated based on the known natural isotopic abundances for $^{14}N/^{15}N$.

Absolute Integral Cross Sections: By using the measured intensity for reactant N_2^+ PFI-PIs and the corrected intensities for product H_2O^+ and N_2H^+ ions, quantum-vibrational-state-selected $\sigma_{CT}(v^+ = 0–2)$ and $\sigma_{HT}(v^+ = 0–2)$ values can be determined based on the Beer–Lambert law, as described in detail previously (Chang et al. 2012; Xu et al. 2013b, 2016).

The k_r values of previous measurements are converted into σ values by using the approximated relation, $k_r = \sigma \langle \nu \rangle$, where $\langle \nu \rangle$ is the averaged ion-molecule collision velocity calculated using the E_{cm}. This relation is also used to convert the σ values obtained here and in previous experiments into k_r values. This conversion scheme enables the comparison of experimental results obtained in dynamics and kinetics measurements as well as in theoretical predictions.

In order to confirm that the $\sigma_{CT}(v^+)$ and $\sigma_{HT}(v^+)$ determined in our experiment are not affected by secondary reactions, we have carefully examined the $\sigma_{CT}(v^+ = 0)$ and $\sigma_{HT}(v^+ = 0)$ at $E_{cm} = 0.04–10.00$ eV for reactions (1) and (2) occurring in the reaction gas cell at H_2O gas pressures ranging from 1.0×10^{-5} to 1.0×10^{-4} Torr. We found that the $\sigma_{CT}(v^+ = 0)$ and $\sigma_{HT}(v^+ = 0)$ curves observed in this H_2O pressure range are in excellent agreement. As an example, we show the comparison of the $\sigma_{CT}(v^+ = 0)$ curves obtained at 4×10^{-5} and 1.0×10^{-4} Torr in Figure 2(a), and those of the $\sigma_{HT}(v^+ = 0)$ curves in Figure 2(b). The fact that the $\sigma_{CT}(v^+ = 0)$ and $\sigma_{HT}(v^+ = 0)$ determined at these pressures are in excellent accord supports the conclusion that the $\sigma_{CT}(v^+ = 0–2)$ and $\sigma_{HT}(v^+ = 0–2)$ curves obtained here are reliable and are only negligibly affected by secondary collision processes.

The $\sigma_{CT}(v^+ = 0–2)$ and $\sigma_{HT}(v^+ = 0–2)$ curves measured in the E_{cm} range of 0.04–10.00 eV are shown in Figures 3(a) and (b), respectively. As shown below, the general trend of the $\sigma_{CT}(v^+ = 0–2)$ curves [$\sigma_{CT}(v^+ = 0–2)$ versus E_{cm} plots] observed at $E_{cm} = 0.04–1.00$ eV is consistent with the long-range near resonant CT mechanism. The $\sigma_{CT}(v^+)$ is very high ($\approx$200 Å^2) at near thermal collision energies ($E_{cm} \approx 0.03–0.04$ eV), and it decreases monotonically as E_{cm} is increased to $\approx$1.00 eV. Most interestingly, the $\sigma_{CT}(v^+ = 0–2)$ curves exhibit a hump at E_{cm} 1.0–5.0 eV, which has not been observed in previous experiments. The $\sigma_{CT}(v^+ = 0–2)$ decreases from the peak of the hump at $E_{cm} \approx 3.0$ eV to near the background level at $E_{cm} = 9.0–10.0$ eV. At $E_{cm} \leqslant 8.0$ eV, the formation of H_2O^+ via CT is the overwhelming product channel with $\sigma_{CT}(v^+) > \sigma_{HT}(v^+)$. However, at $E_{cm} \geqslant 9.0$ eV, $\sigma_{CT}(v^+)$ becomes smaller than $\sigma_{HT}(v^+)$. This observation suggests that the reaction mechanism may switch from near resonant CT to more direct collisional pathways. The decreasing trend for $\sigma_{HT}(v^+ = 0–2)$ observed as E_{cm} is increased, as shown in Figure 3(b), which is in accordance with an exothermic barrier-less reaction process.

The vibrational effects on $\sigma_{CT}(v^+)$ and $\sigma_{HT}(v^+)$ can be examined based on the comparison of the $\sigma_{CT}(v^+ = 0–2)$ and $\sigma_{HT}(v^+ = 0–2)$ curves in Figures 3(a) and (b), respectively. For the CT channel, minor vibrational inhibition effects are discernible at $E_{cm} \leqslant 0.30$ eV, resulting in $\sigma_{CT}(v^+ = 0) > \sigma_{CT}(v^+ = 1) > \sigma_{CT}(v^+ = 2)$. The comparison of Figure 3(b) reveals little vibrational effect for $\sigma_{HT}(v^+)$. The minor v^+-vibrational effect observed here for the $N_2^+(X^2\Sigma_g^+;\ v^+ = 0–2) + H_2O$ reaction is consistent with the minor v^+-excitation effects observed previously for the vibrational-state-selected reactions of $N_2^+(X^2\Sigma_g^+:\ v^+ = 0–2) + CH_4$ (C_2H_2) (Xu et al. 2013a); (Xu et al. 2016).

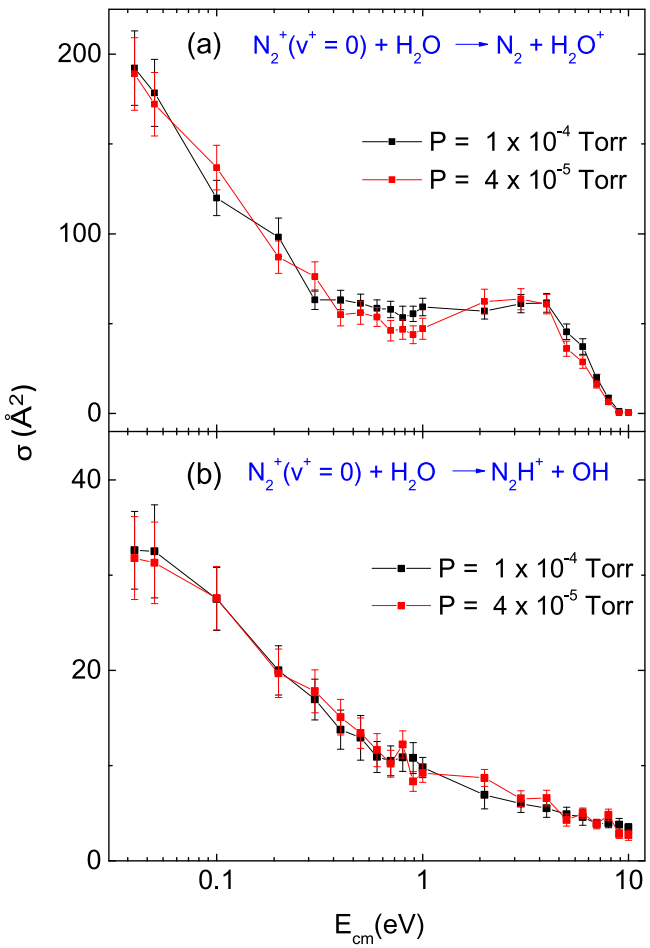

Figure 2. Comparison of (a) the $\sigma_{CT}(v^+ = 0)$ and (b) $\sigma_{HT}(v^+ = 0)$ for the $N_2^+(X^2\Sigma_g^+;\ v^+ = 0) + H_2O$ reaction with the H_2O pressure kept at 4×10^{-5} and 1×10^{-4} Torr in the reaction gas cell. The excellent agreement of the $\sigma_{CT}(v^+ = 0)$ and $\sigma_{HT}(v^+ = 0)$ curves obtained at different H_2O pressures indicates that the $\sigma_{CT}(v^+ = 0\text{–}2)$ and $\sigma_{HT}(v^+ = 0\text{–}2)$ determined in our study are reliable and are not influenced by secondary collisions.

The chemical reactivity of $N_2^+(X^2\Sigma_g^+$: $v^+ = 0\text{–}2)$ toward H_2O can be measured by the sum $\sigma_{SUM}(v^+) = \sigma_{CT}(v^+) + \sigma_{HT}(v^+)$, $v^+ = 0\text{–}2$. The $\sigma_{SUM}(v^+ = 0\text{–}2)$ curves in the range of $E_{cm} = 0.04\text{–}10.00$ eV are depicted in Figure 4. The CT channel being the dominant product channel, the E_{cm} and v^+-vibrational dependences observed for $\sigma_{SUM}(v^+)$ are expected to be similar to those for $\sigma_{CT}(v^+)$. The humps resolved in the $\sigma_{CT}(v^+0\text{–}2)$ curves at $E_{cm} = 1.0\text{–}5.0$ eV are also evident in the $\sigma_{SUM}(v^+ = 0\text{–}2)$ curves of Figure 4. We have included in Figures 3(a), (b), and 4 all previous available experimental σ- and k_r-measurements for comparison with the $\sigma_{CT}(v^+)$, $\sigma_{HT}(v^+)$, and $\sigma_{SUM}(v^+)$ values obtained in our study here. However, we note that all previous σ and k_r measurements are not state-selected studies.

To facilitate the discussion below, we show in Figure 5 the potential energy diagram in the heat-of-formation scale for the reactant states $N_2^+(X^2\Sigma_g^+$: $v^+ = 0$, 1, and 2) + H_2O and the possible product states $H_2O^+(X^2B_1) + N_2(X)$, $N_2H^+(X) + OH(X)$, $H_2O^+(A^2A_1) + N_2(X)$, $H_2O^+(B^2B_2) + N_2(X)$, $OH^+(X) + H + N_2(X)$, and $H^+ + OH(X) + N_2(X)$. On the right side of the potential energy diagram, we have posted the He I photoelectron spectrum of H_2O (Kimura 1981) with the photoionization energy

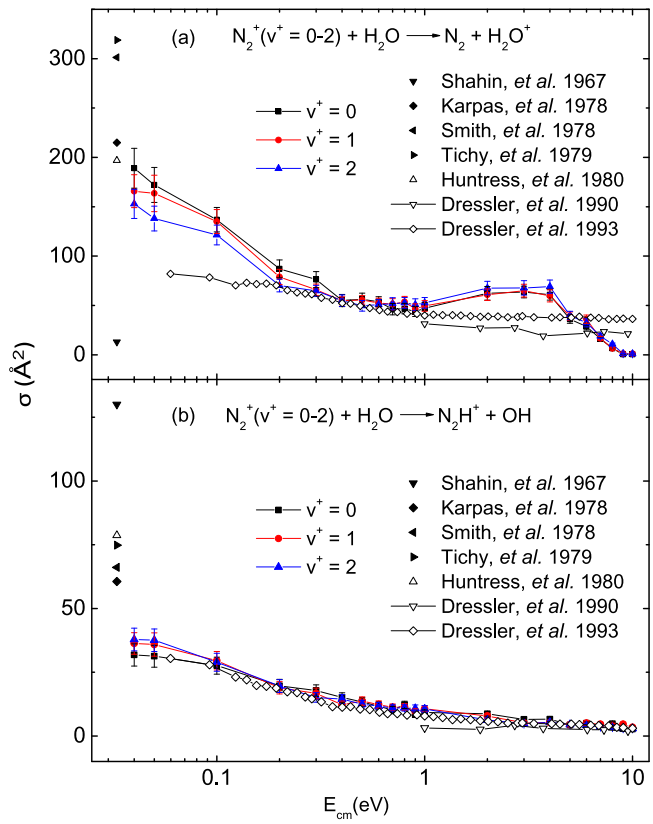

Figure 3. Comparison of (a) the $\sigma_{CT}(v^+ = 0\text{–}2)$ and (b) the $\sigma_{HT}(v^+ = 0\text{–}2)$ curves for the $N_2^+(X^2\Sigma_g^+;\ v^+ = 0\text{–}2) + H_2O$ reaction at $E_{cm} = 0.04\text{–}10.00$ eV. Results from previous kinetics studies near thermal energies and dynamics studies using the crossed-ion-neutral-beam and the rf-octopole ion-guided techniques are also included in the figures. We note that all previous experiments are not state-selected measurements.

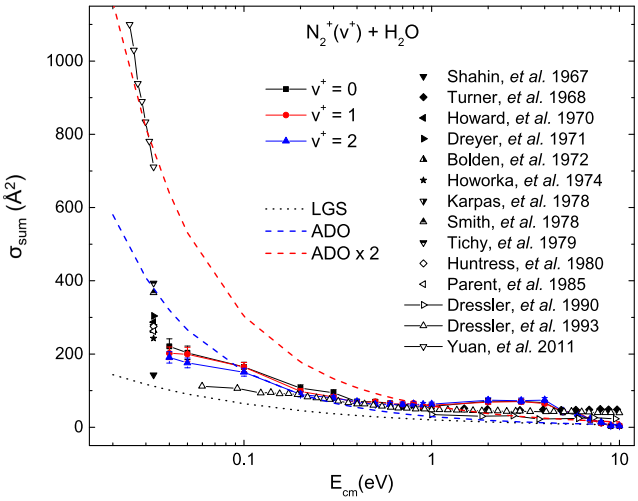

Figure 4. Comparison of the $\sigma_{SUM}(v^+ = 0\text{–}2)$ [$=\sigma_{CT}(v^+ = 0\text{–}2) + \sigma_{HT}(v^+ = 0\text{–}2)$] curves for the $N_2^+(X^2\Sigma_g^+;\ v^+ = 0\text{–}2) + H_2O$ reactions obtained at $E_{cm} = 0.04\text{–}10.00$ eV in our study with those reported previously. Results from previous kinetics studies at near thermal energies and dynamics studies using the crossed-ion-neutral-beam and the rf-octopole ion-guided techniques are also included in the figures. All previous experiments are not state-selected measurements. We have also depicted in the figure the recent rf-ion-trap kinetics measurements obtained at the rotational temperatures of = 222–298 K for comparison with the theoretical σ(ADO) and σ(LGS) predictions.

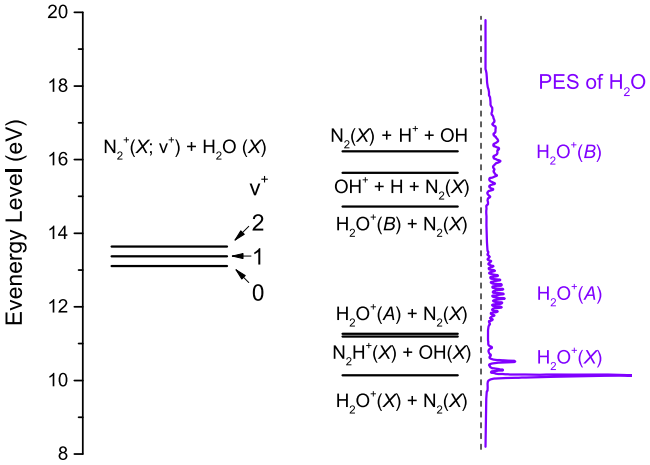

Figure 5. Potential energy diagram in the heat-of-formation scale for the $N_2^+(X^2\Sigma_g^+$: $v^+ = 0$–2) + H_2O reaction system. The heats of formation for the reactant states $N_2^+(X^2\Sigma_g^+$; $v^+ = 0$, 1, and 2) + H_2O and the possible product states $H_2O^+(X^2B_1) + N_2(X)$, $N_2H^+(X) + OH(X)$, $H_2O^+(A^2A_1) + N_2(X)$, $H_2O^+(B^2B_2) + N_2(X)$, $OH^+(X) + H + N_2(X)$, and $H^+ + OH(X) + N_2(X)$ are shown. The He I photoelectron spectrum of H_2O molecule is posted on the right side of the figure. The intensities for the vibronically resolved photoelectron bands are measures of the relative Franck-Condon factors (FCFs) for the corresponding photoionization processes of $H_2O(X)$ to form the $H_2O^+(X$, A, and $B)$ ion states.

scale normalized to the heat-of-formation scale. This He I spectrum covers the formation of the H_2O (X, A, and B) states. The intensities for the vibronically resolved photoelectron bands are measures of the Franck-Condon factors (FCFs) for the corresponding photoionization transitions to form the latter ion states from the $H_2O(X)$ neutral ground state. As shown in Figure 5, at low E_{cm} values, the near energy-resonance CT mechanism is expected to favor the production of excited $H_2O^+(A^2A_1$: $v_1^+v_2^+v_3^+) + N_2$ states that are in energy-resonance with the $N_2^+(X^2\Sigma_g^+$: $v^+ = 0$, 1, and 2) + H_2O reactant states. The formation of excited $H_2O^+(A^2A_1$: $v_1^+v_2^+v_3^+)$ ion states from the $N_2^+(X^2\Sigma_g^+) + H_2O$ CT collisions has been observed in the chemi-luminescence experiment of Dressler and coworkers (Dressler et al. 1990a). Based on the energy diagram of Figure 5, the FCF for the formation of near resonant $H_2O^+(A^2A_1)$: $v_1^+v_2^+v_3^+)$ state is higher from the $N_2^+(X^2\Sigma_g^+$: $v^+ = 0)$ ground state than from the $N_2^+(X^2\Sigma_g^+$; $v^+ \geqslant 1)$ vibrationally excited states, and thus giving rise to minor vibrational inhibition for $\sigma_{CT}(v^+)$, i.e., $\sigma_{CT}(v^+ = 0) > \sigma_{CT}(v^+ = 1) > \sigma_{CT}(v^+ = 2)$ observed at low $E_{cm} \leqslant 0.3$ eV, as shown in Figures 3(a) and 4.

According to known energetic data (Kimura 1981; Reutt et al. 1986; Truong et al. 2009), the energetic threshold for the formation of the $H_2O^+(B^2B_2) + N_2(X)$, state is 1.62 eV above the energy of the $N_2^+(X^2\Sigma_g^+$; $v^+ = 0) + H_2O$ reactant state. This value coincides with the onset at $E_{cm} \approx 1$–2 eV observed for the hump resolved in the $\sigma_{CT}(v^+ = 0$–2) curves of Figure 3(a). Based on this observation, we have identified this hump at $E_{cm} \approx 1.0$–5.0 eV to arise from the formation of excited ions in the $H_2O^+(B^2B_2)$: $v_1^+v_2^+v_3^+)$ state via the collision-assisted CT mechanism for the $N_2^+(X^2\Sigma_g^+$; $v^+ = 0$–2) + H_2O reaction. The hump is found to decline at $E_{cm} \geqslant 4.0$ eV. Two reasons may contribute to the decline: one is the possible dissociation of internally excited $H_2O^+(B^2B_2)$ ions, and the other is that the near energy-resonance CT pathway becomes less important at higher $E_{cm} \geqslant 4.0$ eV. Excited $H_2O^+(B^2B_2)$ ions with internal energies above the OH^+ and H^+ dissociation thresholds are known to result in prompt dissociation (Lorquet & Lorquet 1974; Suárez et al. 2015). The E_{cm} threshold for the lowest dissociation channel, i.e., the formation of $OH^+(X) + H + N_2(X)$ from the $N_2^+(X^2\Sigma_g^+$; $v^+ = 0) + H_2O(X)$ collision, is known to be at 2.54 eV. At higher $E_{cm} \geqslant 3.12$ eV, the dissociation to form $H^+ + OH(X) + N_2(X)$ can also occur. However, as a result of the low OH^+ and H^+ fragment ion intensities, the OH^+ and H^+ ions were not measured in our experiment. Interestingly, a recent lifetime study has shown that at internal excitation below but near the ion dissociation thresholds for the formation of these product ions, the radiative lifetimes of $H_2O^+(B^2B_2$: $v_1^+v_2^+v_3^+)$ ions are surprisingly long with a value of $\approx 200\ \mu$s (Harbo et al. 2014). We note that this lifetime value is within the timescale of our experimental measurements. Therefore, the decline of $\sigma_{CT}(v^+ = 0$–2) observed here may be mainly ascribed to the fast weakening of the near energy-resonance CT processes when $E_{cm} \geqslant 4.0$ eV.

Previous studies of the $N_2^+ + H_2O$ reaction were mostly concerned with k_r measurements near thermal energies ($E_{cm} = 30$–40 meV; Shahin 1967; Turner & Rutherford 1968; Howard et al. 1970; Dreyer & Perner 1971; Bolden & Twiddy 1972; Howorka et al. 1974; Karpas et al. 1978; Smith et al. 1978; Tichý et al. 1979; Huntress et al. 1980; Parent et al. 1985; Dressler et al. 1990b, 1993; Yuan et al. 2011). The σ values obtained in previous dynamics studies (Shahin 1967; Turner & Rutherford 1968; Howard et al. 1970; Dreyer & Perner 1971; Bolden & Twiddy 1972; Howorka et al. 1974; Karpas et al. 1978; Smith et al. 1978; Tichý et al. 1979; Huntress et al. 1980; Parent et al. 1985; Dressler et al. 1990b, 1993; Yuan et al. 2011) or converted from previous reported k_r measurements are included in Figures 3(a), (b), and (4) for comparison with the $\sigma_{CT}(v^+)$, $\sigma_{HT}(v^+)$, and $\sigma_{SUM}(v^+)$, $v^+ = 0$–2 values obtained in our study. These comparisons show that the experimental results of previous kinetics measurements on the $N_2^+ + H_2O$ reaction at near thermal collision energies are widely scattered and lack general agreement. Recently, Gerlich and coworkers (Yuan et al. 2011) have examined the k_r value for the $N_2^+ + H_2O$ reaction by varying the neutral reactant H_2O rotational temperatures in the range of 222–298 K using the rf-ring trap technique, and the σ values (converted from k_r values) thus obtained are significantly higher than all other measurements shown in Figure 4. As discussed below, because of the long-range ion-dipole and charge-induced-dipole interactions for the $N_2^+ + H_2O$ collision pair, the $\sigma_{CT}(v^+)$ values for this reaction are expected to be very high, as confirmed by the experimental measurements of Gerlich and coworkers (Yuan et al. 2011).

Using the crossed-ion-neutral beam method, Turner and Rutherford (Turner & Rutherford 1968) have earlier measured the σ_{CT} and the σ_{HT} as a function of E_{cm} and found that these σ values are nearly independent of E_{cm} in the range of 1–10 eV. The σ_{CT} and σ_{HT} curves measured in the E_{cm} range of 0.06–10 eV have also been reported by Dressler and coworkers (Dressler et al. 1990b, 1993) using the guided ion-beam mass spectrometric technique. These σ_{CT} and σ_{HT} curves thus determined are in fair agreement with the σ values obtained by the crossed-beam experiment at $E_{cm} = 1$–10 eV. As shown in Figures 3(a), (b), and 4, the σ_{CT}, σ_{HT}, and σ_{SUM} curves reported by Turner and Rutherford and Dressler and coworkers are in reasonable agreement with the $\sigma_{CT}(v^+ = 0$–2) $\sigma_{HT}(v^+ = 0$–2) and $\sigma_{SUM}(v^+ = 0$–2) curves observed in our experiment. However, the hump resolved at $E_{cm} = 1.0$–5.0 eV

in the $\sigma_{CT}(v^+ = 0–2)$ and $\sigma_{SUM}(v^+ = 0–2)$ curves was not observed in previous studies. As discussed above, we have tentatively assigned this hump to the formation of excited $H_2O^+(B^2B_2)$ ions by the collision-assisted CT mechanism.

Ion-dipole and Ion-induced Dipole Models: In addition to experimental σ values, theoretical σ predictions based on the Langevin–Gioumousis–Stevenson (LGS; Gioumousis & Stevenson 1958) and the averaged dipole orientation (ADO) models (Su & Bowers 1973a, 1973b) are also depicted in Figure 4 as the black dotted and blue dashed curves, respectively. We found that the $\sigma_{SUM}(v^+ = 0–2)$ curves obtained in this experiment are in reasonable agreement with the σ(ADO) predictions. Two times of the σ(ADO) predictions, i.e., $2 \times \sigma$(ADO), obtained at near thermal energies ($E_{cm} \approx 30–40$ meV) are found to be in excellent agreement with the recent k_r measurements of Gerlich and coworkers (Yuan et al. 2011), and thus the $2 \times \sigma$(ADO) curve (shown as the red dashed curve) is also shown in Figure 4 for comparison with other experimental results.

Since the ADO model includes the prediction of the LGS model, we only list the interaction potential formula (Israelachvili 2011; in SI units) for the ADO model below:

$$V(r) = -\frac{1}{4\pi\varepsilon_0}\frac{e\mu_D\langle\cos(\Theta)\rangle}{r^2} - \left(\frac{1}{4\pi\varepsilon_0}\right)^2\frac{e^2\alpha}{2r^4}. \quad (4)$$

Here $V(r)$, r, ε_0, e μ_D, Θ, and α represent the interaction potential, the center-of-mass distance between N_2^+ and H_2O, the vacuum permittivity constant, the electron charge, the permanent dipole moment of H_2O molecule, the angle between μ_D and r, and the average polarizability of H_2O molecule, respectively, where $\mu_D = 1.8546$ D or 6.19×10^{-30} mC and $\alpha = 1.61 \times 10^{-40}\,\mathrm{kg^{-1}\,s^2\,C^2}$ are known (Nelson et al. 1967; Miller & Bederson 1978). The angle-averaged $\langle\cos(\Theta)\rangle$ value is taken to be 0.5. The first potential term is the interaction between a charge and a permanent dipole, and the second term is for the interaction between a charge and an induced dipole. We note that the LGS model only has the second term.

The σ(ADO) determined based on $V(r)$ can be expressed as follows:

$$\sigma(\mathrm{ADO}) = \pi b_c^2 = \frac{1}{4\varepsilon_0}\frac{e\mu_D\langle\cos(\Theta)\rangle}{E_{cm}} + \frac{1}{4\varepsilon_0}\left(\frac{2e^2\alpha}{E_{cm}}\right)^{1/2}, \quad (5)$$

where b_c is the critical impact parameter. The second term in Equation (5) is the expression of σ(LGS). Equation (5) readily shows that both σ(ADO) and σ(LGS) are predicted to be enhanced dramatically as E_{cm} approaches zero. This increasing trend as E_{cm} is decreased predicted by the σ(ADO) and σ(LGS) models is in fair agreement with the experimental $\sigma_{SUM}(v^+)$ values shown in Figure 4. The majority of previous experimental σ values are found to fall in between the σ(ADO) (blue dashed) and σ(LGS) (black dotted) curves. The kinetics results obtained from the recent study (Yuan et al. 2011) employing the rf-ring trap technique are larger than the ADO predictions at thermal energies by about a factor of two, which might indicate that a more complicated reaction mechanism is involved. We note that only the CT channel was measured in the rf-ring trap study. As shown in Figure 4, the $\sigma_{SUM}(v^+ = 0–2)$ curves at low $E_{cm} < 1.0$ eV are similar to the curve of the σ(ADO) predictions.

The $\sigma_{HT}(v^+)$ decreases smoothly, resulting in a switch of the dominant reaction channel from the CT to the HT channel at $E_{cm} \geqslant 9.00$ eV. At higher E_{cm} region, the direct collision reaction pathways are expected to become more important, which may be responsible for the observed switching of the dominant reaction channels.

Products Branching Ratios: We list in Table 1 detailed BRs for the CT and HT product channels of the $N_2^+(X^2\Sigma_g^+; v^+ = 0–2) + H_2O$ reaction obtained in our study, which were determined by the intensities of product H_2O^+ and N_2H^+ ions measured in the E_{cm} range from 0.04 to 10.00 eV. At $E_{cm} = 0.04–8.00$ eV, the dominant product channel is the CT channel for all vibrational states $N_2^+(v^+ = 0–2)$. It is interesting to find that the BRs of the CT and HT channels are essentially independent of E_{cm} and v^+ at $E_{cm} = 0.04–1.00$ eV with the v^+-averaged $BR(H_2O^+) = 0.82 \pm 0.05$. As E_{cm} is increased from 1.00 eV, the $BR(H_2O^+)$ is found to increase and peak at 0.93 at $E_{cm} = 3.00$ eV. The $BR(H_2O^+)$ drops as E_{cm} is increased beyond 4.00 eV. At $E_{cm} \geqslant 9.00$ eV, the HT product channel, which corresponds to the formation of N_2H^+, becomes dominant compared to the CT channel for all $N_2^+(v^+ = 0–2)$ vibrational states.

Table 2 compares the $BR(H_2O^+)$:$BR(N_2H^+)$ value for the $N_2^+(X^2\Sigma_g^+; v^+) + H_2O$ reaction obtained here with those reported in previous studies (Karpas et al. 1978; Smith et al. 1978; Tichý et al. 1979; Huntress et al. 1980; Dressler et al. 1993) at near thermal energies. The comparison shows that our determinations of $BR(H_2O^+)$:$BR(N_2H^+) = 0.82 \pm 0.05$:$0.18 \pm 0.05$ are in excellent agreement with the $BR(H_2O^+)$:$BR(N_2H^+)$ values of 0.82:0.18 reported by Smith et al. and that of 0.81:0.19 by Tichy et al. obtained by using the selected ion flow tube method. Two other measurements reported the $BR(H_2O^+)$:$BR(N_2H^+)$ values as 0.71:0.29 and 0.73:0.27 by Kappas et al. and Huntress et al. are obtained using the ion-cyclotron mass spectrometric technique. These $BR(H_2O^+)$ values are lower than our measurement by about 15%. The measurement of Dressler and coworkers yield a $BR(H_2O^+)$ value of 0.79, which is found to fall in between of the values obtained by the selected ion flow tube and the ion-cyclotron mass spectrometric methods.

The detailed $BR(H_2O^+)$:$BR(N_2H^+)$ values and $\sigma_{CT}(v^+)$ and $\sigma_{HT}(v^+)$ measurements for the $N_2^+ + H_2O$ reaction determined as a function of both E_{cm} and v^+ vibrational state of reactant N_2^+ are expected to serve as valuable experimental benchmarks for state-of-the-art theoretical chemical dynamics calculations as well as for chemical modeling of planetary atmospheres. Since the intensities of different product ions can be measured simultaneously, the error limits (±5%) achieved for BR measurements are significantly smaller than those (±30%) for $\sigma_{CT}(v^+ = 0–2)$ and $\sigma_{HT}(v^+ = 0–2)$ measurements. Thus, BR data determined here are expected to be better experimental benchmarks for theoretical predictions than $\sigma_{CT}(v^+)$ and $\sigma_{HT}(v^+)$ measurements.

3.2. $H_2O^+(X^2B_1$: $v_1^+v_2^+v_3^+ = 000$ *and* $100) + N_2$

As shown in the potential energy diagram of Figure 5, the energy of the $H_2O^+(X^2B_1$: 000) + N_2 reactant state is the lowest (or most stable) of all the possible open product states. Because of the endothermic constraint, the formation of these product states from the $H_2O^+(X^2B_1$: 000, 100) + N_2 reactant state is low. Thus, we have only measured the σ_{PT}(000 and 100) curves as depicted in Figure 6 for the formation of N_2H^+ from the $H_2O^+(X^2B_1$: 000 and 100) + N_2 reaction. The

Table 1
The Branching Ratios for the Formation of H_2O^+ [BR(H_2O^+)] and N_2H^+ [BR(N_2H+)] via the CT and HT Reaction Channels of the Quantum-vibrational-state-selected Reaction $N_2^+(X^2\Sigma_g^+$: $v^+ = 0$–2) + H_2O in the E_{cm} Range of = 0.04 to 10 eV[a,b]

	$v^+ = 0$		$v^+ = 1$		$v^+ = 2$	
E_{cm}(eV)	BR(H_2O^+)	BR(N_2H^+)	BR(H_2O^+)	BR(N_2H^+)	BR(H_2O^+)	BR(N_2H^+)
0.04	0.86	0.14	0.82	0.18	0.80	0.20
0.05	0.85	0.15	0.82	0.18	0.79	0.21
0.10	0.83	0.17	0.82	0.18	0.81	0.19
0.20	0.82	0.18	0.81	0.19	0.78	0.22
0.30	0.81	0.19	0.80	0.20	0.81	0.19
0.40	0.78	0.22	0.82	0.18	0.79	0.21
0.50	0.81	0.19	0.80	0.20	0.80	0.20
0.60	0.82	0.18	0.81	0.19	0.81	0.19
0.70	0.82	0.18	0.82	0.18	0.82	0.18
0.80	0.79	0.21	0.82	0.18	0.83	0.17
0.90	0.84	0.16	0.83	0.17	0.82	0.18
1.00	0.84	0.16	0.82	0.18	0.83	0.17
2.00	0.88	0.12	0.89	0.11	0.92	0.08
3.00	0.91	0.09	0.93	0.07	0.93	0.07
4.00	0.90	0.10	0.92	0.08	0.93	0.07
5.00	0.89	0.11	0.90	0.10	0.90	0.10
6.00	0.85	0.15	0.88	0.12	0.89	0.11
7.00	0.81	0.19	0.78	0.22	0.84	0.16
8.00	0.57	0.43	0.61	0.39	0.76	0.24
9.00	0.15	0.85	0.22	0.78	0.27	0.73
10.00	0.15	0.85	0.24	0.76	0.24	0.76

Notes.
[a] The BR(H_2O^+) values have been corrected for the formation of secondary H_3O^+ ions from the reaction between product H_2O^+ ions of the $N_2^+(X^2\Sigma_g^+$; $v^+ = 0$–2) + H_2O reactions and neutral H_2O molecules in the gas cell.
[b] The error limits for the BR(H_2O^+) and BR(N_2H^+) are estimated to be 5%.

Table 2
Comparison of the BR(H_2O^+) and BR(H_2O^+) for the Formation of H_2O^+ and N_2H^+ from the $N_2^+(v^+ = 0$–2) + H_2O Reaction Determined at Temperature (T) = 298, 580, and 700 K

	BR(H_2O^+)	BR(N_2H^+)	T(K)[a,b,c]
This work[d]	0.82 ± 0.05	0.18 ± 0.05	580 K
Ref. (Karpas et al. 1978)	0.78	0.22	298 K
Ref. (Smith et al. 1978)	0.82	0.18	298 K
Ref. (Tichý et al. 1979)	0.81	0.19	298 K
Ref. (Huntress et al. 1980)	0.71	0.29	298 K
Ref. (Dressler et al. 1993)	0.73	0.27	700 K

Notes.
[a] $T \approx 580$ K is converted from $E_{cm} = 0.05$ eV.
[b] $T = 298$ K is obtained by assuming that the kinetic measurements were performed at room temperature.
[c] $T \approx 700$ K is converted from $E_{cm} = 0.06$ eV.
[d] The BR(H_2O^+) and BR(N_2H^+) are found to be constant at the E_{cm} range of 0.05–1.00 eV. The values of BR(H_2O^+) = 0.82 ± 0.05 and BR(N_2H^+) = 0.18 ± 0.05 are obtained by averaging the values obtained for the $N_2(v^+ = 0$, 1, and 2) vibrational states as shown in Table 1.

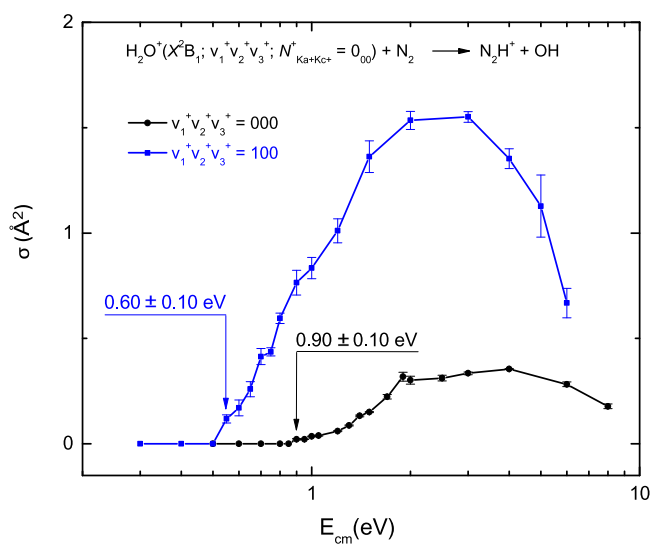

Figure 6. Comparison of the $\sigma_{PT}(000)$ and $\sigma_{PT}(100)$ curves for the formation of N_2H^+ via the PT channel of the $H_2O^+(X^2B_1$: 000 and 100) + N_2 reaction. The distinct E_{cm} thresholds of $\sigma_{PT}(000)$ and $\sigma_{PT}(100)$ were identified at 0.90 ± 0.10 and 0.60 ± 0.10 eV, respectively. The comparison of the $\sigma_{PT}(000)$ and $\sigma_{PT}(100)$ curves reveals a significant (100)-vibrational enhancement.

endothermicity of the process involved means that the $\sigma_{PT}(000$ and 100) values are ten to hundred times lower than those for $\sigma_{CT}(v^+)$ and $\sigma_{HT}(v^+)$, $v^+ = 0$–2, for the $N_2^+(v^+ = 0$–2) + H_2O reaction. As shown in the figure, the $\sigma_{PT}(000$ and 100) curves reveal distinct E_{cm} thresholds at 0.90 ± 0.10 and 0.60 ± 0.10 eV, which can be considered in good agreement with the known thermochemical thresholds of 1.05 ± 0.01 and 0.65 ± 0.01 eV, respectively. The profile of the $\sigma_{PT}(000$ and that of the $\sigma_{PT}(100)$ curves are similar, appearing as a broad peak located at ≈3 eV above the E_{cm} threshold. Most interestingly, the $\sigma_{PT}(100)$ value is found to be greatly enhanced (by about six times) compared to the $\sigma_{PT}(000)$ value. This observation indicates that excitation to the (100) symmetric stretching mode of $H_2O^+(X^2B_1)$ reactant ion is highly effective in driving the endothermic PT reaction channel of the $H_2O^+(X^2B_1)$ + N_2 reaction. Rigorous theoretical dynamics studies based on high level ab initio potential energy

surface calculations are called for to gain further understanding on the reaction mechanism of the titled ion-molecule reaction systems.

4. Conclusions

We have obtained detailed quantum-vibrational-state-selected $\sigma_{CT}(v^+ = 0\text{–}2)$ and $\sigma_{HT}(v^+ = 0\text{–}2)$ measurements for the CT and HT reaction channels of the ion-molecule reaction $N_2^+(X^2\Sigma_g^+; v^+ = 0\text{–}2) + H_2O$ at $E_{cm} = 0.04\text{–}10.00$ eV. Minor vibrational inhibition is observed for the $\sigma_{CT}(v^+ = 0\text{–}2)$ at $E_{cm} = 0.04\text{–}0.30$ eV. The high $\sigma_{CT}(v^+ = 0\text{–}2)$ values along with their decreasing trend observed as E_{cm} is increased suggest that the long-range energy-resonance CT mechanism is operative at low E_{cm} values. We have compared $\sigma_{CT}(v^+ = 0\text{–}2)$ obtained in our experiment with previous dynamics and kinetics measurements and theoretical predictions based on the LGS and ADO models. The $\sigma_{CT}(v^+)$ and $\sigma_{SUM}(v^+)$ measurements resolve a hump in the region of $E_{cm} = 1.0\text{–}5.0$ eV, which was not observed in previous studies. We have tentatively identified this feature to arise from the formation of excited $H_2O^+(B^2B_2)$ ions via the collision-assisted CT excitation mechanism, which is known to have the energetic threshold at $E_{cm} = 1.60$ eV. The $BR(H_2O^+)$ and $BR(N_2H^+)$ values measured as a function of both E_{cm} and v^+ vibrational state of reactant N_2^+ ion are also presented and compared with previous measurements. At $E_{cm} = 0.04\text{–}1.00$ eV, the dominant product ion is H_2O^+ and the $BR(H_2O^+)$ is found to be independent of E_{cm} and v^+-vibrational state with the v^+-averaged value $BR(H_2O^+) = 0.82 \pm 0.05$. As E_{cm} is increased from 1.00 eV, the $BR(H_2O^+)$ increases to the peak value of 0.93 at $E_{cm} = 3.00$ eV. At $E_{cm} > 4.00$ eV, the $BR(H_2O^+)$ further decreases as E_{cm} is increased, and eventually becomes lower than the $BR(N_2H^+)$ at $E_{cm} \geqslant 9.00$ eV, where direct collision reaction dynamics may play a more dominant role.

In order to gain further insights into the titled reaction systems, we have also performed σ measurements for the $H_2O^+(X^2B_1$: 000 and 100) + N_2 reaction. In the E_{cm} range of interest, only the formation of N_2H^+ from the PT reaction channel of the latter reaction is observed. The σ_{PT}(000 and 100) curves thus obtained exhibit distinct E_{cm} thresholds, which agree with the corresponding thermochemical thresholds. Furthermore, the $\sigma_{PT}(100)$ values are found to be nearly six times higher than the $\sigma_{PT}(000)$ values, which is indicative of a significant vibrational enhancement effect for excitation to the (100) symmetric stretching mode of $H_2O^+(X^2B_1)$. The detailed $\sigma_{CT}(v^+ = 0\text{–}2)$, $\sigma_{HT}(v^+ = 0\text{–}2)$, $\sigma_{SUM}(v^+ = 0\text{–}2)$ and σ_{PT}(000 and 100) as well as branching ratios $BR(H_2O^+)$:$BR(N_2H^+)$ reported here are expected to serve as valuable benchmarks for the development of a state-of-the-art theoretical chemical dynamics package.

This material is based upon work supported by the National Science Foundation under CHE-1462172 and CHE-1763319. C.Y.N. is also grateful to Dr. Huie Tarng Liou for his generous donation of research support for the Ng Laboratory.

ORCID iDs

Cheuk-Yiu Ng https://orcid.org/0000-0003-4425-5307

References

Bolden, R. C., & Twiddy, N. D. 1972, Faraday Discuss. Chem. Soc., 53, 192
Chang, Y. C., Xu, H., Xu, Y., et al. 2011, JChPh, 134, 201105
Chang, Y. C., Xu, Y., Lu, Z., Xu, H., & Ng, C. Y. 2012, JChPh, 137, 104202
Chantry, P. J. 1971, JChPh, 55, 2746
Dressler, R. A., Gardner, J. A., Lishawa, C. R., Salter, R. H., & Murad, E. 1990a, JChPh, 93, 9189
Dressler, R. A., Gardner, J. A., Salter, R. H., Wodarczyk, F. J., & Murad, E. 1990b, JChPh, 92, 1117
Dressler, R. A., Salter, R. H., & Murad, E. 1993, JChPh, 99, 1159
Dreyer, J. W., & Perner, D. 1971, CPL, 12, 299
Ervin, K. M., & Armentrout, P. B. 1985, JChPh, 83, 166
Giguere, P., & Huebner, W. 1978, ApJ, 223, 638
Gioumousis, G., & Stevenson, D. P. 1958, JChPh, 29, 294
Harbo, L. S., Dziarzhytski, S., Domesle, C., et al. 2014, PhRvA, 89, 052520
Herbst, E. 2001, Chemical Society Reviews, 30, 168
Howard, C. J., Rundle, H. W., & Kaufman, F. 1970, JChPh, 53, 3745
Howorka, F., Lindinger, W., & Varney, R. N. 1974, JChPh, 61, 1180
Huntress, W., Jr., Anicich, V., McEwan, M., & Karpas, Z. 1980, ApJS, 44, 481
Israelachvili, J. N. 2011, Intermolecular and Surface Forces (New York: Academic)
Karpas, Z., Anicich, V., & Huntress, W. 1978, CPL, 59, 84
Kimura, K. 1981, Handbook of He I Photoelectron Spectra of Fundamental Organic Molecules: Ionization Energies, ab initio Assignments, and Valence Electronic Structure for 200 Molecules (Tokyo: Japan Scientific Societies Press)
Larsson, M., Geppert, W. D., & Nyman, G. 2012, RPPh, 75, 066901
Li, A., Li, Y., Guo, H., et al. 2014, JChPh, 140, 011102
Lorquet, A. J., & Lorquet, J. C. 1974, CP, 4, 353
Miller, T. M., & Bederson, B. 1978, AdAMP, 13, 1
Nelson, R. D., Jr, Lide, D. R., Jr., & Maryott, A. A. 1967, Selected Values of Electric Dipole Moments for Molecules in the Gas Phase (Washington, DC: National Bureau of Standards)
Parent, D. C., Derai, R., Mauclaire, G., et al. 1985, CPL, 117, 127
Qian, X.-M., Zhang, T., Chang, C., et al. 2003, RScI, 74, 4096
Reutt, J. E., Wang, L. S., Lee, Y. T., & Shirley, D. A. 1986, JChPh, 85, 6928
Ruscic, B., Feller, D., & Peterson, K. A. 2013, Theoretical Chemistry Accounts, 133, 1415
Semo, N. M., & Koski, W. S. 1984, JPhCh, 88, 5320
Shahin, M. M. 1967, JChPh, 47, 4392
Smith, D. 1992, ChRv, 92, 1473
Smith, D., Adams, N. G., & Miller, T. M. 1978, JChPh, 69, 308
Smith, D., & Spanel, P. 1995, MSRv, 14, 255
Snow, T. P., & Bierbaum, V. M. 2008, ARAC, 1, 229
Song, H., Li, A., Guo, H., et al. 2016, PCCP, 18, 22509
Su, T., & Bowers, M. T. 1973a, IJMSI, 12, 347
Su, T., & Bowers, M. T. 1973b, JChPh, 58, 3027
Suárez, J., Méndez, L., & Rabadán, I. 2015, JPhCh, 6, 72
Tanaka, K., Durup, J., Kato, T., & Koyano, I. 1981, JChPh, 74, 5561
Tichý, M., Rakshit, A. B., Lister, D. G., et al. 1979, IJMSI, 29, 231
Truong, S. Y., Yencha, A. J., Juarez, A. M., et al. 2009, CP, 355, 183
Turner, B. R., & Rutherford, J. A. 1968, JGR, 73, 6751
Williams, K. L., Martin, I. T., & Fisher, E. R. 2002, JASMS, 13, 518
Xiong, B., Chang, Y.-C., & Ng, C.-Y. 2017a, PCCP, 19, 18619
Xiong, B., Chang, Y.-C., & Ng, C.-Y. 2017b, PCCP, 19, 29057
Xu, Y., Chang, Y. C., Lu, Z., & Ng, C. Y. 2013a, ApJ, 769, 72
Xu, Y., Xiong, B., Chang, Y.-C., et al. 2017a, PCCP, 19, 9778
Xu, Y., Xiong, B., Chang, Y. C., & Ng, C. Y. 2012, JChPh, 137, 241101
Xu, Y., Xiong, B., Chang, Y. C., & Ng, C. Y. 2013b, JChPh, 139, 024203
Xu, Y., Xiong, B., Chang, Y. C., & Ng, C. Y. 2016, ApJ, 827, 17
Xu, Y., Xiong, B., Chang, Y. C., & Ng, C. Y. 2017b, PCCP, 19, 8694
Yuan, B., Scott, Z., Tikhonov, G., Gerlich, D., & Smith, M. A. 2011, JPCA, 115, 25